Faraday Discussions

Cite this: *Faraday Discuss.*, 2020, **223**, 278

ROYAL SOCIETY OF CHEMISTRY

PAPER

View Article Online
View Journal | View Issue

Characterization and possible function of an enigmatic reflector in the eye of the shrimp *Litopenaeus vannamei*

Nathan Schiffmann,[a] Eyal Merary Wormser,[b] Vlad Brumfeld,[c] Yoseph Addadi,[d] Iddo Pinkas,[c] Venkata Jayasurya Yallapragada,[e] Eliahu D. Aflalo,[fg] Amir Sagi,[fh] Benjamin A. Palmer,†*[a] Steve Weiner[a] and Lia Addadi*[a]

Received 23rd April 2020, Accepted 11th May 2020

DOI: 10.1039/d0fd00044b

Reflective assemblies of high refractive index organic crystals are used to produce striking optical phenomena in organisms based on light reflection and scattering. In aquatic animals, organic crystal-based reflectors are used both for image-formation and to increase photon capture. Here we report the characterization of a poorly-documented reflector in the eye of the shrimp *L. vannamei* lying 150 μm below the retina, which we term the proximal reflective layer (PR-layer). The PR-layer is made from a dense but disordered array of polycrystalline isoxanthopterin nanoparticles, similar to those recently reported in the tapetum of the same animal. Each spherical nanoparticle is composed of numerous isoxanthopterin single crystal plates arranged in concentric lamellae around an aqueous core. The highly reflective plate faces of the crystals are all aligned tangentially to the particle surface with the optical axes projecting radially outwards, forming a birefringent spherulite which efficiently scatters light. The nanoparticle assemblies form a broadband reflective sheath around the screening pigments of the eye, resulting in pronounced eye-shine when the animal is viewed from a dorsal-posterior direction, rendering the eye pigments inconspicuous. We assess possible functions of the PR-layer and conclude that it likely functions as a camouflage device to conceal the dark eye pigments in an otherwise largely transparent animal.

[a]*Department of Structural Biology, Weizmann Institute of Science, Rehovot, 7610001, Israel. E-mail: bpalmer@bgu.ac.il; Lia.Addadi@weizmann.ac.il*

[b]*Department of Chemical Engineering, Ben-Gurion University of the Negev, Beer-Sheva, 8410501, Israel*

[c]*Department of Chemical Research Support, Weizmann Institute of Science, Rehovot, 7610001, Israel*

[d]*Department of Life Sciences Core Facilities, Weizmann Institute of Science, Rehovot, 7610001, Israel*

[e]*Department of Physics of Complex Systems, Weizmann Institute of Science, Rehovot, 7610001, Israel*

[f]*Department of Life Sciences, Ben-Gurion University of the Negev, 8410501, Beer-Sheva, Israel*

[g]*Department of Life Sciences, Achva Academic College, Arugot, Israel*

[h]*The National Institute for Biotechnology in the Negev, Ben-Gurion University of the Negev, Beer-Sheva, 8410501, Israel*

† Present address: Department of Chemistry, Ben-Gurion University of the Negev, Beer-Sheva, Israel.

Introduction

Small aquatic animals face major challenges associated with seeing underwater. Firstly, the reduced refractive index contrast between water and the internal eye tissues means that lenses are less effective. This is particularly true for small eyes, where short focal-distances mean that extremely high-powered lenses would be required to focus light onto the retina. The sensitivity of eyes with such minute apertures is also extremely low.[1] Secondly, for transparent pelagic animals such as larval crustaceans, the eye pigments necessary for vision are often the most prominent feature of the animal that could attract the attention of predators. Organisms have evolved ingenious strategies to resolve both these obstacles, often involving the use of reflectors. In many aquatic animals, reflectors are used instead of lenses to form images.[1] These mirrored eyes are both compact and extremely efficient at collecting light.[2,3] One example is the scallop eye, which produces images by reflecting light from a concave mirror onto the overlying retina.[4,5] Similar concave-mirrored eyes are found in deep-sea fish[6,7] and crustaceans.[8]

The reflective superposition eye of decapod crustaceans also uses reflectors for its operation.[9,10] Each compound eye is composed of thousands of square-faceted eye units (the ommatidia) and usually contains two types of reflectors:[10,11] (i) the image-forming 'distal mirror' in the upper part of the ommatidia, which focuses light onto the retina (comprising the photosensitive rhabdoms), and (ii) the intensity-enhancing 'tapetum' underlying the retina which back-scatters light onto the rhabdoms, giving them a second chance to capture photons not absorbed on the first pass. Some of the photons reflected by the tapetum are transmitted back out of the eye, resulting in 'eye-shine' when crustacean eyes are illuminated and observed along the eye axis.[12] The upper image-forming apparatus and photosensitive rhabdom layer are separated by an unpigmented zone which allows light entering numerous corneal facets to be superimposed onto a single rhabdom, effectively increasing the eyes' aperture. This leads to a huge increase in sensitivity over apposition eyes where each ommatidium acts as an independent optical unit.[13] Superposition optics thus confer a considerable advantage over apposition optics in low-light habitats.[14]

While the majority of adult decapod crustaceans possess reflecting compound superposition eyes,[13] apposition eyes are found in all larval decapods.[15] The apposition eye is suited to the brighter environments of the larvae's planktonic habitat and thus, image-forming and intensity-enhancing reflectors are absent from these eyes.[16] However, larval decapods, which are often almost completely transparent, use reflectors to conceal opaque eye pigments as a means of remaining inconspicuous,[17] thus retaining the ability to *see* and avoid being *seen*.

Many biological reflectors used in both color production[18–22] and vision[3] are constructed from highly reflective assemblies of organic crystals. These photonic devices are often made from multilayer stacks of crystals interspersed with cytoplasm in the form of a Bragg reflector. Light reflects at the interface between the high (crystal) and low (cytoplasm) refractive index materials by constructive interference.[20,23] Recently, we have also discovered 3-dimensional photonic crystals constructed from periodic arrays of crystalline nanoparticles.[24] In both the Bragg reflector and 3D photonic crystal systems, the proportion of the light

reflected increases as the refractive index contrast between the low and high medium increases. Indeed, in the systems that have been fully characterized, the component organic crystals guanine,[25] isoxanthopterin[26] and 7,8-dihydroxanthopterin[27] have exceptionally high refractive indices along one crystallographic axis, between 1.8–2.0. In the case of guanine and isoxanthopterin the high refractive indices (1.83 and 1.96, respectively), are a product of their crystal structures formed from layers of planar hydrogen-bonded isoxanthopterin molecular arrays.[26]

The reflectors in decapod crustacean eyes are made of crystalline isoxanthopterin.[26] The tapetum reflector, which encapsulates the base of photosensing rhabdoms, is formed from 3-dimensional assemblies of polycrystalline nanoparticles, each comprised of numerous isoxanthopterin single crystal plates. The component crystal plates are all aligned tangentially to the particle surface, forming an anisotropic onion-like structure with a hollow core.[24,26] During a recent study of the eyes of the Pacific whiteleg shrimp *L. vannamei*,[24] we observed that in addition to the distal mirror and tapetum found in most decapods, *L. vannamei* possesses another reflector underlying the tapetum, which we term the 'proximal reflective layer' (PR-layer). Furthermore, we also observed that *L. vannamei* exhibits more pronounced eye-shine than other decapods when observed from almost any angle of incidence (Fig. 1). We hypothesized that the PR-layer may be the cause of this enhanced eye-shine. The presence of a reflective layer proximal to the tapetum was first noted by Welsh[28] and Kleinholz[29] in the 1930's and later by Zyznar,[30] but was poorly characterized and its function remained a mystery. Here, we perform a comprehensive characterization of the chemical and structural properties of the PR-layer and assess its possible functions.

Results

To investigate the 3D organization of the reflective structures in the eye of *L. vannamei* (Fig. 1), we performed X-ray micro-CT measurements on the dark-adapted adult eye (Fig. 2A). The 3D organization of the eye is similar to that observed in other decapods.[26] Two regions of high X-ray attenuation appear in the upper part of the eye: the cornea and the distal mirror.[26] The high X-ray attenuation of the cornea is likely due to the presence of calcium carbonate,[31] while the

Fig. 1 The shrimp *L. vannamei* with its protruding eyes and conspicuous eye-shine under white light illumination. Inset: a higher magnification view of the left eye, which displays distinct eye-shine even when viewed from a dorsal-posterior direction.

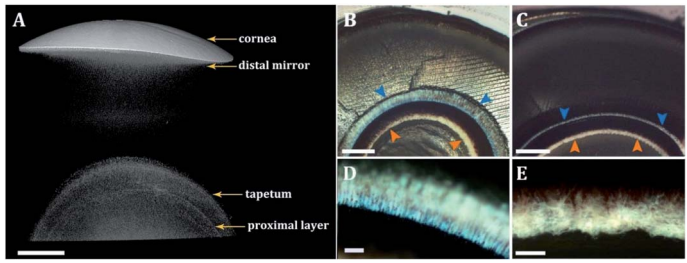

Fig. 2 (A) X-ray micro-CT of an adult, dark-adapted, *L. vannamei* eye. (B–E) Polarized light microscopy images of dark- and light-adapted adult eyes. (B) and (C) Longitudinal section of dark-adapted (B) and light-adapted (C) eyes. Blue and orange arrowheads mark the location of the tapetum and the proximal reflective layer, respectively. (D) and (E) Higher magnification longitudinal sections of the tapetum (D) and proximal layer (E). Scale bars: A = 500 μm, B, C = 200 μm, D, E = 50 μm.

attenuation of the distal mirror originates from the crystalline reflecting material it contains.[26] The 'clear zone', a region of low contrast analogous to the vitreous body of mammalian eyes, separates the distal mirror from a third area of high X-ray contrast in the lower part of the eye, the tapetum, which also contains reflecting material.[24] In addition to these components, which are well-documented features of reflecting superposition compound eyes,[26] a fourth area of high X-ray contrast is observed about 150 μm below the tapetum (Fig. 2). This area appears as a thin layer located proximal and parallel to the curved tapetum.

Polarized light micrographs of longitudinal sections through the eye (parallel to the eye axis) show that the distinctly blue, birefringent tapetum is arranged in columns about 100 μm long (Fig. 2B and D). These columns form a close sheath around the photosensitive rhabdoms, optically isolating each rhabdom from its neighbor (Fig. 2D).[24,26] A white, highly birefringent reflecting layer is observed 150 μm below the tapetum (Fig. 2B–E), which corresponds to the position of the high contrast feature observed proximal to the tapetum in X-ray CT. We refer to this layer as 'the proximal reflecting layer' (abbreviated to PR-layer). The 70 μm-thick PR-layer comprises birefringent, fibrous-like elements exhibiting protrusions that extend upwards into the absorbing pigment (Fig. 2E). The birefringence of the tapetum and PR-layer suggests they are composed of crystalline materials. Importantly, between the tapetum and the PR-layer, a 150 μm-thick region of absorbing pigment prevents light impinging along the eye-axis from reaching the PR-layer. There is no significant change in the appearance of the PR-layer upon light-adaptation. However, following light-adaptation, the tapetum narrows to a 50 μm-thick layer. This narrowing of the tapetum results either from a contraction of its reflective material or by motile absorbing pigments invading the layer.

In order to identify the birefringent materials found in the eyes of *L. vannamei*, we recorded Raman spectra from the PR-layer and compared them to the known composition of the tapetum[26] and the interlaying absorbing pigment. We obtained a spectrum characteristic of isoxanthopterin both from the tapetum and from the PR-layer (Fig. 3). Spectra acquired from the absorbing pigment did not display the Raman signature of isoxanthopterin.

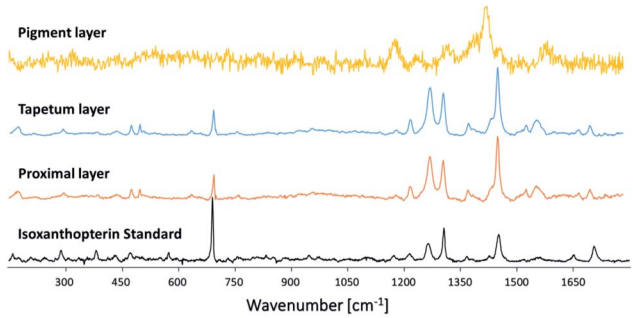

Fig. 3 Raman spectra recorded from the *L. vannamei* pigment layer, tapetum and PR-layer, together with the Raman spectrum of crystalline isoxanthopterin.

In order to map the isoxanthopterin contained in the tapetum and PR-layer and to locate the position of the PR-layer relative to the other eye components, we relied on the intrinsic fluorescence of the isoxanthopterin molecule (excitation maximum, $\lambda = 340$ nm; emission maximum, $\lambda = 400$ nm).[32] Eye sections stained with the nucleus stain DAPI were imaged with a widefield microscope using the DAPI filter, capturing the DAPI emission and isoxanthopterin fluorescence in the same channel. Both the tapetum and the PR-layer exhibit strong fluorescence signals (Fig. 4A), which overlap with the birefringent regions observed by polarizing microscopy (Fig. 4B). This confirms that isoxanthopterin is a major component of the tapetum and PR-layer. The tapetum displays the ordered pattern of the retina, whereas the PR-layer has a fibrous-like texture. Moreover, the PR-layer is located just above a dense layer of DAPI-stained nuclei. This nuclei-rich layer can be identified as the lamina ganglionaris – the first optic ganglion in the visual pathway.[33]

We then used two-photon excitation microscopy to obtain high-resolution images of the fibrous-like texture of the PR-layer, exciting at the absorption maximum of isoxanthopterin at 340 nm. The images show that the PR-layer contains fibers with a thickness of 1–3 μm, typically tens of micrometers long (Fig. 4C). Within the middle of the layer the fibers are oriented parallel to the eye

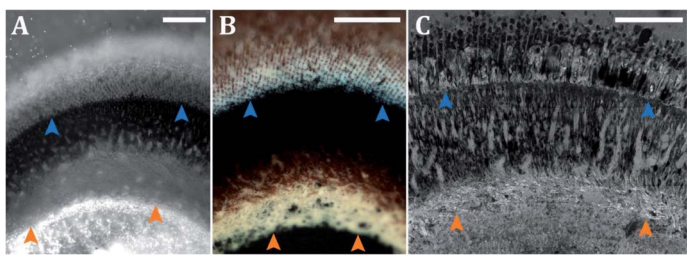

Fig. 4 Fluorescence microscopy imaging of the tapetum and PR-layer. (A) Widefield fluorescence microscopy of a DAPI stained eye section comprising the tapetum and PR-layer. (B) Polarized light microscopy of an eye section of similar orientation to (A). (C) Two-photon excitation microscopy of an unstained eye section comprising the tapetum and PR-layer. Blue and orange arrowheads mark the location of the tapetum and PR-layers, respectively. Scale bars: A, B, C = 200 μm.

curvature, but at the distal edge (towards the tapetum) they have a perpendicular orientation (Fig. 4C). Whether the fibers are composed of isoxanthopterin, or whether the isoxanthopterin is organized around the fibers, cannot be determined. We note that tiny packets of white, birefringent matter can be resolved within the PR-layer, suggesting it contains a crystalline material (Fig. 4C).

Based on the location of the PR-layer determined by light microscopy, we obtained cryo-SEM images of the region located 150 μm below the tapetum in a longitudinal eye section. Spherical nanoparticles, with an average diameter of 374 nm (±37 nm, $n = 152$), are arranged either in dense arrays along fiber bundles, or in small packets inside membrane-bound organelles (Fig. 5A–C). Each elongated fiber bundle contains tens of fibers 17–20 nm in diameter and several micrometers long. The nanoparticles appear identical to the crystalline isoxanthopterin particles observed previously in the tapetum of several decapods, including *L. vannamei*.[24,26] The PR-layer nanoparticles are also composed of numerous polygonal (100) single crystal plates (*ca.* 50 × 50 × 10 nm) arranged in concentric lamellae around an aqueous core (Fig. 5D). The nanoparticles are densely distributed, although no periodic order is observed as in the tapetum.[24]

To investigate the optical properties of the reflective layers in *L. vannamei*, we measured the back-scattering from the tapetum, the underlying absorbing pigment and the PR-layer. Using an optical microscope and illuminating small areas from within these regions, we collected the scattered light with a high NA objective. The tapetum spectrum exhibits much higher back-scattering towards the blue end of the spectrum, whereas the PR-layer exhibits more broadband scattering with slightly higher scattering efficiency at blue wavelengths (Fig. 6). In the part of the visible spectrum which is relevant to the light environment of *L. vannamei* (wavelengths up to 550 nm), the tapetum is a stronger reflector than the PR-layer. As expected from the light micrographs of the eye sections, the absorbing pigment layer back-scatters light only at the red end of the spectrum (Fig. 6). Consequently, the pigment layer absorbs all the light at wavelengths up to 550 nm and must appear black in the shrimp's light environment.

The 150 μm-thick region of absorbing pigment is located between the tapetum and the PR-layer. Thus, light impinging along the eye-axis cannot reach the PR-layer, suggesting that it does not have a visual function. To assess possible

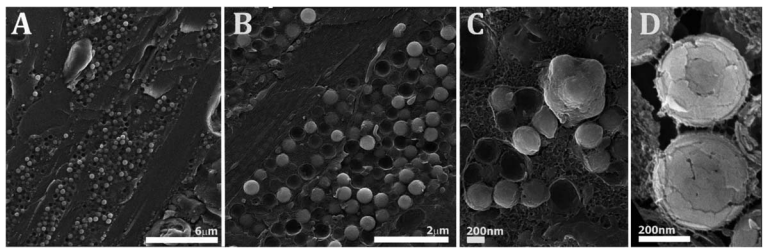

Fig. 5 Cryo-SEM imaging of the ultrastructure of the PR-layer comprising crystalline isoxanthopterin nanoparticles. (A) Low-magnification view of the PR-layer, comprising nanoparticles arranged either in dense arrays along fiber bundles, or in small packets inside membrane-bound organelles. (B) The nanoparticles from the fiber bundle region. (C) The nanoparticles from the small membrane-bound organelles. (D) Higher magnification of the spherical nanoparticles.

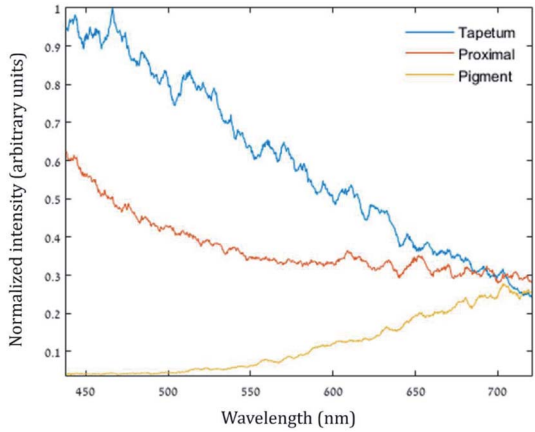

Fig. 6 *In situ* back-scattering measurements of the tapetum, pigment layer and PR-layer. All the spectra were divided by the source spectrum (measured with a silver mirror) to obtain a qualitative understanding of the variation of reflectivity with wavelength.

functions of the PR-layer we tracked its formation during development, to determine if there is a correlation between the emergence of the reflector and the changing behavioral patterns of *L. vannamei* during ontogeny. We investigated early (Zoea-2 larva) and late (Postlarva-4) stages of eye development. The 5 dpf (days post-fertilization) zoea-2 larva is mostly pigmented (Fig. 7A) and possesses an apposition eye where, below the cornea, the crystalline cones lead directly onto the photosensitive rhabdoms which are surrounded by screening pigment (Fig. 7B and C).[34] Using X-ray micro-CT we identified corneal lens facets of polygonal shape located at the top of the few ommatidia which constitute the eye (Fig. 8A). In the longitudinal section, we do not observe any regions of high contrast that could be attributable to dense crystalline structures such as the tapetum or PR-layer (Fig. 8B).

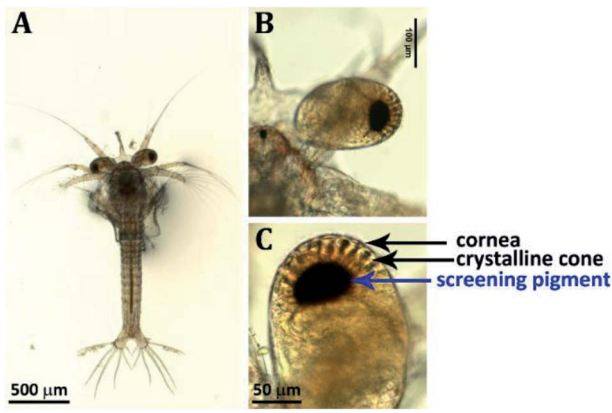

Fig. 7 Light microscopy of the zoea-2 larva eye. (A) A whole zoea-2 larva. (B) The zoea-2 larva apposition eye. (C) Visual part of the zoea-2 larva apposition eye with components identified.

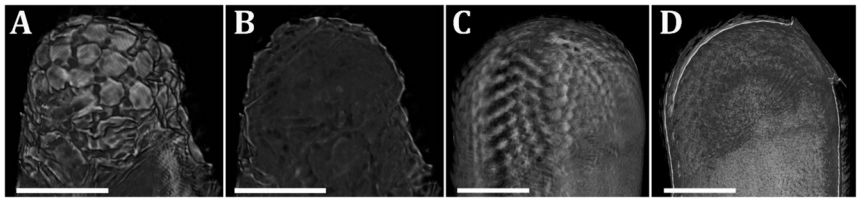

Fig. 8 X-ray micro-CT of *L. vannamei* zoea-2 and postlarva-4 eyes. (A) and (B) X-ray micro-CT of a zoea-2 larva eye showing the corneal surface (A) and longitudinal section (B) views. (C) and (D) X-ray micro-CT of a postlarva-4 eye showing the surface (C) and longitudinal section (D) views. The isotropic voxel size in the reconstructed volumes of both scans is 0.5 μm. Scale bars: A, B = 50 μm; C, D = 100 μm.

The 15 dpf postlarva-4 shrimp is also mostly pigmented and possesses a larger apposition eye (Fig. 9A). In the lower, less pigmented part of the eye stalk, the optic ganglia are seen as oval opaque bodies (Fig. 9B, red arrowheads). In addition to the cornea and crystalline cones, below the screening pigment and elongated rhabdoms, the transverse layer of the lamina ganglionaris is found (the first optic ganglion) (Fig. 9C). Micro-CT imaging of the postlarva-4 eye demonstrates the hexagonal shape of the corneal lens facets (Fig. 8C), which is characteristic of apposition eyes.[16] In longitudinal sections we observe a region of high X-ray attenuation located 50 μm below the cornea, which corresponds to the location of the rhabdoms and resembles them in appearance (Fig. 8D).

In order to further investigate the region at high resolution we imaged the postlarva-4 eye using cryo-SEM. Since the eye is small it can be imaged as a whole (Fig. 10A). The rhabdoms extend from the bottom of the crystalline cone towards the inner part of the eye (Fig. 10B; green and blue squares, respectively). Between the cross-sectioned rhabdoms (easily recognizable due to the regular

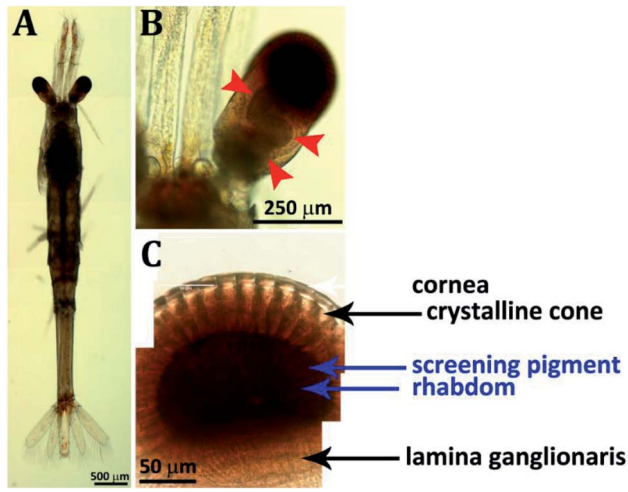

Fig. 9 Light microscopy of the postlarva-4 eye. (A) Whole postlarva-4 *L. vannamei*. (B) The postlarva-4 apposition eye. Red arrowheads mark the location of optic ganglia. (C) Visual part of the postlarva-4 apposition eye with components identified.

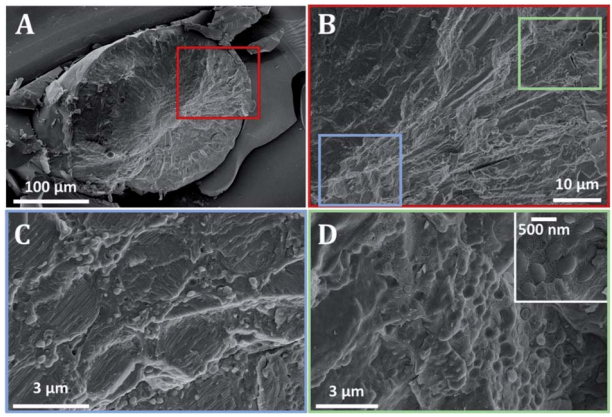

Fig. 10 Cryo-SEM images of the postlarva-4 eye. (A) Low-magnification view of a whole eye. The red box marks the region shown in (B). (B) The region comprising the rhabdoms. The blue box denotes an area at the bottom of the rhabdoms shown in (C). The green box denotes an upper region of the rhabdom shown in (D), including an inset showing the texture of the particles found around the rhabdoms at high resolution.

arrangement of microvilli) are round to oval particles, ~400 nm in diameter (Fig. 10C). These particles are also present in the upper part of the rhabdoms (Fig. 10D). At higher magnification, the particles exhibit a smooth external and internal texture (Fig. 10D inset), which is reminiscent of the appearance of pigment granules.[26] The smooth texture of the particles is very different from the crystalline isoxanthopterin nanoparticles in the adult tapetum, that are not observed in the postlarva-4 eye. Consequently, we do not identify a tapetum or a PR-layer in the postlarva-4 eye.

Discussion

Chemical, structural and optical properties of the PR-layer

The PR-layer underlying the tapetum was first observed in the shrimp *P. vulgaris* by Welsh[28] and Kleinholz[29] in the 1930's and later by Zyznar in *L. setiferus*.[30] However, these reports were inconclusive and contradictory regarding its structure, content and function. The PR-layer in *L. vannamei* is a white, birefringent structure located 150 μm below the retina just above the lamina ganglionaris. We show that it is composed of polycrystalline isoxanthopterin nanoparticles, similar in size and structure to those recently reported in the tapetum.[24] The spherical nanoparticles are composed of numerous isoxanthopterin single crystal plates arranged in concentric lamellae around an aqueous core. In the tapetum the nanoparticles are densely packed in organized, periodic arrays that envelop and optically isolate each rhabdom.[24] In contrast, the packing of the nanoparticles in the PR-layer is less organized, and they are arranged in arrays along fiber bundles or in small packets inside intra-cellular membrane-bound organelles. This results in a disorganized fibrous-like microstructure.

Previous studies showed that the tapetum isoxanthopterin nanoparticles exhibit remarkable optical properties, resulting from their unique structural arrangement.[24,35] The component isoxanthopterin crystal plates are aligned with

their *a* axes projecting radially away from the surface of the sphere, forming a spherically symmetric, birefringent particle. The high in-plane refractive index ($n = 1.96$) of the component isoxanthopterin crystals is thus oriented tangentially to the particle surface, enhancing the refractive index contrast between the shell and the core. It was shown that individual birefringent particles back-scatter twice as much light as equivalent isotropic particles, due to the variation of the refractive index within the particle shell.[24] Similarly, the reflectivity from periodic assemblies of birefringent particles (as observed in the tapetum) is significantly enhanced in comparison to assemblies of isotropic particles[24] and results from the higher refractive index modulation in the birefringent arrays.

The PR-layer exhibits relatively weak scattering throughout the visible spectrum, with stronger scattering at the blue end of the spectrum. The tapetum is a much more efficient reflector and displays an increased propensity for scattering blue light. The broader-band and weaker scattering of the PR-layer presumably results from a reduced degree of order in the packing and particle size distribution in comparison to the tapetum. The tapetum exhibits densely packed, periodic particle arrays and, in contrast to the PR-layer, there is a contribution of both specular reflectance and scattering to the bulk optical behavior. This results in an enhancement in the measured back-scattering intensity. Interestingly, both the tapetum and the PR-layer preferentially reflect the blue light that penetrates the *L. vannamei* habitat (up to 70 m depth[36]), matching the spectral sensitivity of the shrimp's photoreceptors[34] (400–550 nm). Indeed, in many visual systems which use reflectors to produce images[5] or to increase light-sensitivity,[24,26,27] the peak in reflectivity spectrum spectrally matches the light environment of the organism's habitat.

Assessing the function of the PR-layer

Whilst the function of the tapetum is well-established, previous reports could not establish the function of the PR-layer due to a lack of understanding of its structure and composition. Based on our results, we examine several possibilities for its function.

The PR-layer is separated from the retina by 150 μm of absorbing pigment, meaning no light impinging along the eye's optic axis will reach it. This precludes a function directly related to vision. Furthermore, the absence of the reflector in larvae and postlarvae shrimp rules out the hypothesis that the adult PR-layer is a non-functional 'vestige' of a previously-functional optical device. Welsh[28] and Kleinholz[29] suggested that the PR-layer was a proximal extension of the tapetum, containing a reservoir of motile reflecting pigment (thought to be guanine) that migrates distally towards the tapetum in the dark, and retracts proximally upon light-adaptation. However, our microscopy results show that there are no significant changes in the structure of the PR-layer between dark- and light-adapted states. In both states, the tapetum and PR-layers are separated by a thick region of screening pigment, and there is no continuity between these layers. This agrees with Zyznar's report on *L. setiferus* which suggested that the reflector is a separate tissue with a standalone function.[30]

We suggest that the PR-layer acts as a camouflage device to conceal the eye pigments. In contrast to the majority of crustacean decapods, the adult *L. vannamei* is almost completely lacking in body pigmentation, apparently using

'transparency' as a strategy to remain inconspicuous in the open water.[13,37] The most conspicuous features of the animal are the eye pigments,[13] which include the photo-pigments[38] and the screening pigment required for light–dark adaptation.[13] Pigmented eyes present an obvious predation risk to transparent crustaceans,[39] which have evolved elaborate strategies for concealing eye pigments, mainly based on transparency and light reflection.[17] For example, the apposition eyes of transparent planktonic crustaceans such as hyperiid amphipods[40,41] and the water flea *L. kindtii*[42] contain long crystalline cones without a pigment shield and a small compressed retina, minimizing the visibility of the eye pigments to predators or prey.[13] Many transparent pelagic crustacean larvae, like those of the Stomatopoda, possess a blue/green reflector overlying the opaque screening pigments which sit between photoreceptors.[17] The resulting blueish eyeshine is thought to conceal the conspicuous pigments in the otherwise transparent bodies. In the grass shrimp *P. pugio*, a reflecting pigment found in the retina is concentrated dorsally in larvae and ventrally in adults. Since larvae swim upside-down, the reflecting pigment is oriented downward in all developmental stages and may function as countershading.[39]

In the case of *L. vannamei*, when viewed along the eye's visual axis, the screening pigment which underlies the retina[13] is concealed by the bluish eye-shine of the tapetum. Additionally, light impinging from a dorsal-posterior direction through the transparent eye stalk is also prevented from reaching the absorbing pigment by the enveloping PR-layer (Fig. 1 and 2). As a result, *L. vannamei* exhibits pronounced eye-shine when viewed from almost any angle of incidence (Fig. 1), which renders the eye pigments inconspicuous. These observations are consistent with the hypothesis that the PR-layer functions as a camouflage device to "prevent the eyes from appearing as large dark spots on the otherwise relatively well camouflaged animal".[43] Our hypothesis is strengthened by the fact that the shrimp *P. vulgaris*[28,29] and *L. setiferus*,[30] which also contain a PR-layer, are both transparent animals living in the open ocean and possess transparent eyestalks. Conversely, pigmented freshwater animals such as the crayfish *P. clarkii* (unpublished work) and *C. quadricarinatus* and the freshwater prawn *M. rosenbergii*,[26] which would not benefit from such camouflage, do not possess a PR-layer. The PR-layer is also absent from the highly pigmented larvae and post-larvae of *L. vannamei*, where, similarly, a camouflaging PR-layer would be of no use. To test our hypothesis, future research is required to compare the conspicuity of the eyes in animals possessing a PR-layer and in animals devoid of it in the light environments of their native habitats.

Finally, isoxanthopterin crystals have now been found in the eyes of crustaceans belonging to the Reptantia (the crayfish *P. clarkii* and *C. quadricarinatus*), Caridea (the prawn *M. rosenbergii*[26]) and, most distantly, the Dendrobranchiata (the shrimp *L. vannamei*) suborders of Decapoda.[44] This establishes that crystalline isoxanthopterin is widespread in the decapod crustaceans. The Decapoda is a family of the Malacostraca – the largest class of crustaceans.[45] Interestingly, Zyznar and Nicol identified isoxanthopterin in the eyes of a stomatopod (*S. empusa*) and an isopod (*L. exotica*),[46] two distantly related Malacostraca animals. This suggests that isoxanthopterin may be used as a reflecting material in a variety of optical systems and calls for an investigation of the presence and function of isoxanthopterin crystals in the Malacostraca and in the crustacean group more widely.

Conclusions

We present a characterization of the structural and optical properties of an unexplored reflector – the PR-layer, present in the eyes of some decapod crustaceans. We suggest that the PR-layer functions as a camouflage device to conceal conspicuous eye pigments in the transparent animal – a predator evasion strategy. The eyes of *L. vannamei*, which contain three independent reflectors used for image-formation, enhancing photon capture and camouflage, illustrate the richly diverse functions of organic crystalline materials in vision. The work calls for further exploration of the distribution, functions and formation mechanisms of high refractive index organic crystals in biology.

Materials and methods

Specimen collection and preparation

Adult specimens of *L. vannamei* were grown and maintained at the Ben-Gurion University of the Negev aqua facility under the following conditions: water temperature was maintained at 27 ± 1 °C. The dark/illumination photoperiod was arranged as 12 h light/12 h dark. Food comprised shrimp pellets (30% protein; Rangen) *ad libitum* three times a week. Water quality was assured by circulating the entire water volume through a biofilter maintaining all of the required water physicochemical parameters: pH 8.3 ± 0.5, nitrite <0.1 mg L^{-1}, nitrate <50 mg L^{-1}, ammonium levels were negligible, and oxygen levels were >5 mg L^{-1}. Dark-adapted: *L. vannamei* specimens were maintained under complete dark conditions overnight (dark-adaptation) before eyestalk collection. Light-adapted: *L. vannamei* specimens were maintained under light conditions overnight (light-adaptation) before eyestalk collection. All animals were anesthetized in ice-cold water before dissection. For dark-adapted specimens, the eyestalks were removed from the animal under red illumination to maintain the eyes in the dark-adapted state. The eyestalks were then fixed for 24 h in 4% paraformaldehyde and 2.5% glutaraldehyde in 0.1 M cacodylate buffer, or alternatively in 4% paraformaldehyde in 1× phosphate-buffered saline (PBS), in the dark. After fixation, the cornea was removed manually using a scalpel. For the X-ray micro-CT experiments, the fixed eyestalks were measured without the removal of the cornea. For all the other imaging experiments (light, DAPI fluorescence and confocal microscopy; Raman microspectroscopy; cryo-SEM; back-scattering *in situ* measurements), following the removal of the cornea, sections were obtained by embedding the fixed eyestalks in 7% agar (using 1× PBS as the medium) and cut into 200 μm thick longitudinal and tangential sections (parallel and perpendicular to the ommatidial axis, respectively), using a vibratome (OTS 400; EMS).

Developmental stages of *L. vannamei*, including zoea-2 and the postlarva-4, were obtained from the Maof HaNegev Fish and Shrimps R&D center hatchery. Developmental stage identification was carried out based on the specimens' morphology according to Kitani's classification.[47] The whole animals were fixed immediately after removal from the hatchery in 4% paraformaldehyde in 1× PBS. The animals were kept whole in fixative until the eyestalks were dissected from the animals just before their use for experimentation. For the X-ray micro-CT experiments, the whole fixed eyestalks were measured. For the light microscopy, Raman microspectroscopy and cryo-SEM experiments, sections were

obtained by embedding the fixed eyestalks in 7% agar (using 1× PBS as the medium) and cut into 100 μm thick longitudinal and horizontal sections (parallel and perpendicular to the eye axis, respectively) using a vibratome (VT1000-S; Leica).

Light microscopy

Light microscopy and polarized light microscopy imaging of fixed eye sections was performed using a Nikon Eclipse E600WPOL microscope equipped with a Nikon Digital Sight DS-Fi1-U2 camera in reflection, transmission, or polarization mode with 2.5×, 5×, 10×, 20× and 50× air objectives.

Micro-CT imaging

Micro-CT scans were acquired using Xradia 400 (Zeiss) and Xradia Versa 520 (Zeiss) instruments. Whole eyestalks were placed in a plastic pipette tip, which had been sealed by melting using a flame. To prevent dehydration of the sample, the tips were partially filled with water and the eye was held above the water in a saturated water vapor atmosphere. The tomographic volumes were obtained by taking 1600 projections (180 degrees) at 30 kV and 2 W, with optical magnification of either 4× (for adult specimens) or 20× (for developmental stage specimens). The isotropic voxel sizes in the reconstructed volumes were 2.4 μm and 0.5 μm, respectively. Avizo software (Thermo Fisher Scientific) was used for 3D visualization and analysis.

Raman spectroscopy

The eye sections were placed on a microscope slide for the Raman measurements. Raman measurements were conducted on a LabRAM HR Evolution instrument (Horiba) configured with four laser lines (325, 532, 632, and 785 nm), allowing for Raman spectra from 50 cm^{-1} onward. The instrument was equipped with an 800 mm spectrograph, a CCD detector and a 1024 × 256 pixel open electrode front illuminated CCD camera cooled to −60 °C. The pixel spacing was 1.3 cm^{-1} when working with a 600 grooves per mm grating at 632.8 nm excitation. The sample was exposed to light by various objectives (MPlanFL N NA-0.9, 100×, LUMPLFLN NA-1.0 60XW, and LMPlanFL N NA-0.5 50× LWD; Olympus). The system was set around an open confocal microscope (BXFM Olympus) with a spatial resolution >1 μm when using the 100× objective. The sample was placed upon a software-controlled motorized stage to measure the Raman spectral maps. Most of the analyses were performed with the 632.8 nm HeNe laser, 600 grooves per mm grating, and 100× objective.

DAPI staining and widefield fluorescence microscopy

In a cold room, the eye sections were permeabilized with Triton X-100 (0.1% in PBS, Sigma-Aldrich) for 30 minutes, washed 3 times with PBS, incubated with DAPI (10 μg ml^{-1} in PBS, Sigma-Aldrich) in darkness and washed again 3 times with PBS. The stained eye sections were imaged by a DMi8 widefield fluorescence microscope (Leica-microsystems CMS GmbH, Germany) with inverted configuration with a 10× objective, using the fixed DAPI filter cube (excitation at 400 nm, detection at 450 nm), thus recording the DAPI emission and the tail of the

isoxanthopterin fluorescence in the same channel. LAS X (Leica) software was used for data visualization and analysis.

Two-photon excitation microscopy

The eye sections were imaged by a TCS SP8 Confocal – MultiPhoton microscope (Leica-microsystems CMS GmbH, Germany) with upright configuration, equipped with a Chameleon Vision II – Coherent tunable ultra-fast Ti:Sapphire laser 680–1080 nm, 3 internal spectral detectors and 3 NDD detectors. Excitation was performed at 680 nm with the Ti:Sapphire laser, given that the isoxanthopterin absorption peak is at 340 nm. Emission was recorded by a HyD1 hybrid detector with detection range 380–432 nm, thus including the isoxanthopterin emission peak at 410 nm. The volume was acquired with a HC PL APO 20X/0.75 CS2 objective × objective lens magnification, with z steps of 0.7 μm. The final voxel size was $x = 252$ nm, $y = 252$ nm, $z = 709$ nm. LAS X and ImageJ (U. S. National Institutes of Health) software were used for data visualization and analysis.

Cryo-SEM imaging

The eye sections were cut to size, sandwiched between two metal discs (3 mm in diameter, 0.1 mm cavities), and cryoimmobilized in a 10% dextran solution as cryo-protectant in a high-pressure freezing device (EM ICE; Leica). The frozen samples were mounted on a holder under liquid nitrogen and transferred to a freeze-fracture device (BAF60; Bal-Tec) using a vacuum cryotransfer device (VCT 100; Bal-Tec). Specimens were then taken to the cryo-SEM, etched for 5–10 min at −105 °C, and transferred back to the freeze-fracture device to be coated with 4 nm of Pt. Samples were observed in an Ultra 55 SEM (Zeiss) using a secondary electron in-lens detector, maintaining the frozen-hydrated state with a cryostage operating at a temperature of −120 °C. Measurements of the crystalline nanoparticle diameters were performed from the cryo-SEM micrographs on the nanoparticles that appeared to be at the fracture surface, using ImageJ software.

Back-scattering *in situ* measurements

Back-scattering of light was measured *in situ* directly from eye sections using a previously developed custom built microscope.[19] A small area of the tapetum was illuminated with white light from a xenon lamp, and the resulting scattering was collected with a high numerical aperture (NA) objective. Spectra were obtained using a fiber coupled spectrometer (Shamrock SR303i; Andor) equipped with a iDus 420 CCD cooled camera. The spectra were divided by the source spectrum (measured with a silver mirror), to obtain a qualitative understanding of the variation of reflectivity with wavelength.

Author contributions

L. A., S. W., N. S., and B. A. P. designed and directed the study. V. J. Y. performed the scattering measurements. N. S. and E. M. S. prepared the samples for cryo-SEM and performed polarized microscopy measurements. B. A. P. and N. S. performed cryo-SEM measurements. V. B. and N. S. performed the X-ray micro CT measurements and analysis. I. P. performed the Raman spectroscopy. Y. A. undertook the fluorescence microscopy and two-photon microscopy experiments.

A. S. and E. D. A. provided the specimens and knowledge of shrimp biology. B. A. P., N. S., and L. A. wrote the manuscript with contributions from all the authors.

Conflicts of interest

The authors declare no competing interests.

Acknowledgements

This work was supported by Israel Science Foundation Grants 354/18 and 583/17, the Crown Center of Photonics and ICORE: The Israeli Center of Research Excellence 'Circle of Light'. L. A. is the incumbent of the Dorothy and Patrick Gorman Professorial Chair of Biological Ultrastructure. B. A. P. is the recipient of the 2019 Azrieli Faculty Fellowship and 2019 European Research Council 'CRYSTALEYES' Starting Grant. I. P. is the incumbent of the Sharon Zuckerman research fellow chair.

References

1 M. F. Land and D.-E. Nilsson, *Animal Eyes*, Oxford University Press Inc., New York, 2012.
2 M. F. Land, Eyes with mirror optics, *J. Opt. A: Pure Appl. Opt.*, 2000, **2**, R44.
3 B. A. Palmer, D. Gur, S. Weiner, L. Addadi and D. Oron, The organic crystalline materials of vision: structure-function considerations from the nanometer to the millimeter scale, *Adv. Mater.*, 2018, **30**, 1800006.
4 M. F. Land, Image formation by a concave reflector in the eye of the scallop, *Pecten maximus*, *J. Physiol.*, 1965, **179**, 138–153.
5 B. A. Palmer, G. J. Taylor, V. Brumfeld, D. Gur, M. Shemesh, N. Elad, A. Osherov, D. Oron, S. Weiner and L. Addadi, The image-forming mirror in the eye of the scallop, *Science*, 2017, **358**, 1172–1175.
6 H.-J. Wagner, R. H. Douglas, T. M. Frank, N. W. Roberts and J. C. Partridge, A novel vertebrate eye using both refractive and reflective optics, *Curr. Biol.*, 2009, **19**, 108–114.
7 J. C. Partridge, R. H. Douglas, N. J. Marshall, W. S. Chung, T. M. Jordan and H.-J. Wagner, Reflecting optics in the diverticular eye of a deep-sea barreleye fish (*Rhyncochohyalus natalensis*), *Proc. R. Soc. B*, 2014, **281**, 20133223–9.
8 A. Andersson and D.-E. Nilsson, Fine structure and optical properties of an ostracode (Crustacea) nauplius eye, *Protoplasma*, 1981, **107**, 361–374.
9 K. Vogt, *Zeitschrift für Naturforschung C*, 1975, **30**, 691.
10 M. F. Land, Superposition images are formed by reflection in the eyes of some oceanic decapod crustacea, *Nature*, 1976, **263**, 764–765.
11 M. F. Land, Optics and vision in invertebrates, in *Handbook of Sensory Physiology VII/6B*, ed. H.-J. Autrum, Springer, Berlin, 1981, pp. 471–592.
12 D. G. Stavenga, Pseudopupils of compound eyes, in *Comparative physiology and evolution of vision in invertebrates*, Springer, 1979, pp. 357–439.
13 D.-E. Nilsson, Optics and evolution of the compound eye, in *Facets of vision*, Springer, 1989, pp. 30–73.
14 T. W. Cronin, Optical Design and Evolutionary Adaptation in Crustacean Compound Eyes, *J. Crustacean Biol.*, 1986, **6**, 1–23.

15 E. Gaten, Optics and phylogeny: is there an insight? The evolution of superposition eyes in the Decapoda (Crustacea), *Contributions to Zoology*, 1998, **67**, 223–236.
16 D.-E. Nilsson, Refractive Index Gradients Subserve Optical Isolation in a Light-Adapted Reflecting Superposition Eye, *J. Exp. Zool.*, 1983, **225**, 161–165.
17 K. D. Feller and T. W. Cronin, Hiding opaque eyes in transparent organisms: a potential role for larval eyeshine in stomatopod crustaceans, *J. Exp. Biol.*, 2014, **217**, 3263–3273.
18 T. M. Jordan, J. C. Partridge and N. W. Roberts, Disordered animal multilayer reflectors and the localization of light, *J. R. Soc., Interface*, 2014, **11**, 20140948.
19 D. Gur, B. A. Palmer, B. Leshem, D. Oron, P. Fratzl, S. Weiner and L. Addadi, The mechanism of color change in the Neon Tetra fish: a light-induced tunable photonic crystal array, *Angew. Chem., Int. Ed.*, 2015, **54**, 12426–12430.
20 E. J. Denton, Review lecture: on the organization of reflecting surfaces in some marine animals, *Philos. Trans. R. Soc., B*, 1970, **258**, 285–313.
21 D. Gur, B. Leshem, M. Pierantoni, V. Farstey, D. Oron, S. Weiner and L. Addadi, Structural basis for the brilliant colors of the Sapphirinid copepods, *J. Am. Chem. Soc.*, 2015, **137**, 8408–8411.
22 D. Gur, B. A. Palmer, S. Weiner and L. Addadi, Light manipulation by guanine crystals in organisms: biogenic scatterers, mirrors,multilayer reflectors and photonic crystals, *Adv. Funct. Mater.*, 2017, **27**, 1603514.
23 M. F. Land, The physics and biology of animal reflectors, *Prog. Biophys. Mol. Biol.*, 1972, **24**, 75–106.
24 B. A. Palmer, V. J. Yallapragada, N. Schiffmann, E. M. Wormser, N. Elad, E. D. Aflalo, A. Sagi, S. Weiner, L. Addadi and D. Oron, A highly reflective biogenic photonic material from core–shell birefringent nanoparticles, *Nat. Nanotechnol.*, 2020, **15**, 138–144.
25 A. Hirsch, D. Gur, I. Polishchuk, D. Levy, B. Pokroy, A. J. Cruz-Cabeza, L. Addadi, L. Kronik and L. Leiserowitz, "Guanigma": the revised structure of biogenic anhydrous guanine, *Chem. Mater.*, 2015, **27**(24), 8289–8297.
26 B. A. Palmer, A. Hirsch, V. Brumfeld, E. D. Aflalo, I. Pinkas, A. Sagi, S. Rosenne, D. Oron, L. Leiserowitz, L. Kronik, S. Weiner and L. Addadi, Optically functional isoxanthopterin crystals in the mirrored eyes of decapod crustaceans, *Proc. Natl. Acad. Sci. U. S. A.*, 2018, **115**, 2299–2304.
27 G. Zhang, A. Hirsch, G. Shmul, L. Avram, N. Elad, V. Brumfeld, I. Pinkas, Y. Feldman, R. B. Asher, B. A. Palmer, L. Kronik, L. Leiserowitz, S. Weiner and L. Addadi, Guanine and 7,8-dihydroxanthopterin reflecting crystals in the Zander fish eye: crystal locations, compositions, and structures, *J. Am. Chem. Soc.*, 2019, **141**, 19736–19745.
28 J. H. Welsh, The nature and movement of the reflecting pigment in the eyes of crustaceans, *J. Exp. Zool.*, 1932, **62**, 173–183.
29 L. Kleinholz, Crustacean eye-stalk hormone and retinal pigment migration, *Biol. Bull.*, 1936, **70**(2), 159–184.
30 E. S. Zyznar, *A new catoptric system in the eyes of penaeid shrimp*, 1970.
31 F. I. Alagboso, C. Reisecker, S. Hild and A. Ziegler, Ultrastructure and mineral composition of the cornea cuticle in the compound eyes of a supralittoral and a marine isopod, *J. Struct. Biol.*, 2014, **187**, 158–173.

32 Y. Q. Wang, L. J. Tang and T. Tan, Simultaneous determination of xanthopterin and isoxanthopterin in human urine by synchronous fluorescence spectroscopy, *J. Fluoresc.*, 2010, **20**, 1191–1198.
33 H.-K. Chang, C.-C. Lin and S.-L. Hsuan, Histological and histochemical investigation of the compound eye of the whiteleg shrimp (Litopenaeus vannamei), *PeerJ Preprints*, 2017, 3453v1.
34 K. Matsuda and M. N. Wilder, Difference in light perception capability and spectral response between juveniles and sub-adults of the whiteleg shrimp *Litopenaeus vannamei* as determined by electroretinogram, *Fish. Sci.*, 2010, **76**, 633–641.
35 V. J. Yallapragada and D. Oron, Optical properties of spherulite opals, *Opt. Lett.*, 2019, **44**, 5860–5863.
36 L. Holthuis, Shrimps and prawns of the world. An annotated catalogue of species of interest to fisheries, FAO species catalogue, *FAO Fisheries Synopsis*, 1980, vol. 125, pp. 1–271.
37 M. J. McFall-Ngai, Crypsis in the pelagic environment, *Am. Zool.*, 1990, **30**, 175–188.
38 T. H. Goldsmith, The natural history of invertebrate visual pigments, in *Photochemistry of vision*, Springer, 1972, pp. 685–719.
39 J. K. Douglass and R. B. Forward, The ontogeny of facultative superposition optics in a shrimp eye: hatching through metamorphosis, *Cell Tissue Res.*, 1989, **258**(2), 289–300.
40 M. Land, Optics of the eyes of phronima and other deep-sea amphipods, *J. Comp. Physiol.*, 1981, **145**, 209–226.
41 D.-E. Nilsson, The transparent compound eye of Hyperia (Crustacea): Examination with a new method for analysis of refractive index gradients, *J. Comp. Physiol.*, 1982, **147**(3), 339–349.
42 D.-E. Nilsson, R. Odselius and R. Elofsson, The compound eye of Leptodora kindtii (Cladocera), *Cell Tissue Res.*, 1983, **230**, 401–410.
43 D.-E. Nilsson and H. L. Nilsson, Eye camouflage in the isopod crustacean Astacillalongicornis (Sowerby), *J. Exp. Mar. Biol. Ecol.*, 1983, **68**, 105–110.
44 S. Richter and G. Scholtz, Phylogenetic analysis of the Malacostraca (Crustacea), *J. Zool. Syst. Evol. Res.*, 2001, **39**, 113–136.
45 J. K. Lowry and H. E. Stoddart, *Zoological Catalogue of Australia 19.2B. Crustacea: Malacostraca: Peracarida: Amphipoda, Cumacea, Mysidacea*, CSIRO Publishing, 2003.
46 E. S. Zyznar and J. A. C. Nicol, Ocular reflecting pigments of some malacostraca, *J. Exp. Mar. Biol. Ecol.*, 1971, **6**, 235–248.
47 H. Kitani, Larval Development of the White Shrimp Penaeus vannamei BOONE Reared in the Laboratory and the Statistical Observation of its Naupliar Stages, *Bull. Jpn. Soc. Sci. Fish.*, 1986, **52**, 1131–1139.